BIOCHEMISTRY
including biophysical chemistry & molecular biology

Accelerated Publication

pubs.acs.org/biochemistry

The Specialized Hsp70 (HscA) Interdomain Linker Binds to Its Nucleotide-Binding Domain and Stimulates ATP Hydrolysis in Both *cis* and *trans* Configurations

T. Reid Alderson,[†,∥] Jin Hae Kim,[‡,⊥] Kai Cai,[†,‡] Ronnie O. Frederick,[‡] Marco Tonelli,[§] and John L. Markley*[,†,‡]

[†]Department of Biochemistry, [‡]Mitochondrial Protein Partnership, Center for Eukaryotic Structural Genomics, and [§]National Magnetic Resonance Facility at Madison, University of Wisconsin—Madison, Madison, Wisconsin 53706, United States

Supporting Information

ABSTRACT: Proteins from the *isc* operon of *Escherichia coli* constitute the machinery used to synthesize iron−sulfur (Fe−S) clusters for delivery to recipient apoproteins. Efficient and rapid [2Fe-2S] cluster transfer from the holo-scaffold protein IscU depends on ATP hydrolysis in the nucleotide-binding domain (NBD) of HscA, a specialized Hsp70-type molecular chaperone with low intrinsic ATPase activity (0.02 min^{-1} at 25 °C, henceforth reported in units of min^{-1}). HscB, an Hsp40-type cochaperone, binds to HscA and stimulates ATP hydrolysis to promote cluster transfer; however, while the interactions between HscA and HscB have been investigated, the role of HscA's interdomain linker in modulating ATPase activity has not been explored. To address this issue, we created three variants of the 40 kDa NBD of HscA: NBD alone ($HscA_{386}$), NBD with a partial linker ($HscA_{389}$), and NBD with the full linker ($HscA_{395}$). We found that the rate of ATP hydrolysis of $HscA_{395}$ (0.45 min^{-1}) is nearly 15-fold higher than that of $HscA_{386}$ (0.035 min^{-1}), although their apparent affinities for ATP are equivalent. $HscA_{395}$, which contains the full covalently linked linker peptide, exhibited intrinsic tryptophan fluorescence and basal thermostability that were higher than those of $HscA_{386}$. Furthermore, $HscA_{395}$ displayed narrower $^{1}H^{N}$ line widths in its two-dimensional $^{1}H-^{15}N$ TROSY-HSQC spectrum in comparison to $HscA_{386}$, indicating that the peptide in the *cis* configuration binds to and stabilizes the NBD. The addition to $HscA_{386}$ of a synthetic peptide with a sequence identical to that of the interdomain linker ($L^{387}LLDVIPLS^{395}$) stimulated its ATPase activity and induced widespread NMR chemical shift perturbations indicative of a binding interaction in the *trans* configuration.

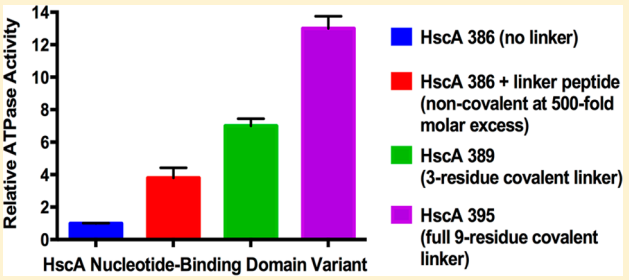

Iron−sulfur (Fe−S) clusters comprise an ancient class of enzymatic cofactors whose biosynthesis occurs in a tightly regulated and intricately complex manner, despite their chemical simplicity (e.g., [2Fe-2S] or [4Fe-4S]) and spontaneous *in vitro* syntheses.[1,2] Proteins that utilize Fe−S clusters (Fe−S proteins) occur throughout nature and are commonly found in essential metabolic (e.g., mitochondrial complex III and aconitase) and biosynthetic (e.g., DNA helicases and polymerases) pathways.[3] Because Fe−S proteins are synthesized in their apo form, they require post-translational insertion of clusters to yield mature, holoenzymes. However, because of the toxicity of iron ions and sulfide and the instability of free Fe−S clusters, cells have evolved dedicated proteinaceous machinery to safeguard cluster synthesis and delivery to recipient apo-Fe−S proteins.[4] This machinery minimizes the level of cytotoxic reactive oxygen species (ROS) that can inflict irreversible macromolecular and cellular damage.[5]

Prokaryotes contain an iron−sulfur cluster (ISC) assembly system that leads to the maturation of nearly all Fe−S proteins under basal cellular conditions.[4] In eukaryotes, the homologous mitochondrion-based ISC assembly system includes more than 30 proteins that function together to cause the maturation of both mitochondrial Fe−S proteins and, with assistance from the cytosolic iron−sulfur cluster assembly (CIA) system, nonmitochondrial (i.e., cytosolic, nuclear, and endoplasmic reticulum-based) Fe−S proteins.[6] Because of the prevalence and biological significance of many Fe−S proteins, defects in Fe−S cluster biosynthesis and delivery manifest as a myriad of human diseases, including Friedreich's ataxia, the most common recessive ataxia.[7,8] Moreover, recent evidence suggests that dysfunctional Fe−S cluster biogenesis could play a potential role in the onset and progression of Parkinson's disease.[9] To understand the biological basis of Fe−S cluster-related human diseases, elucidation of the molecular mechanisms that underlie Fe−S cluster assembly and transfer will prove to be critical. Many research groups over the past 15 years have utilized the ISC assembly proteins of *Escherichia coli* as a model system for investigating the structural and biophysical details of Fe−S cluster biogenesis.[10] Because of

Received: August 21, 2014
Revised: October 30, 2014
Published: November 5, 2014

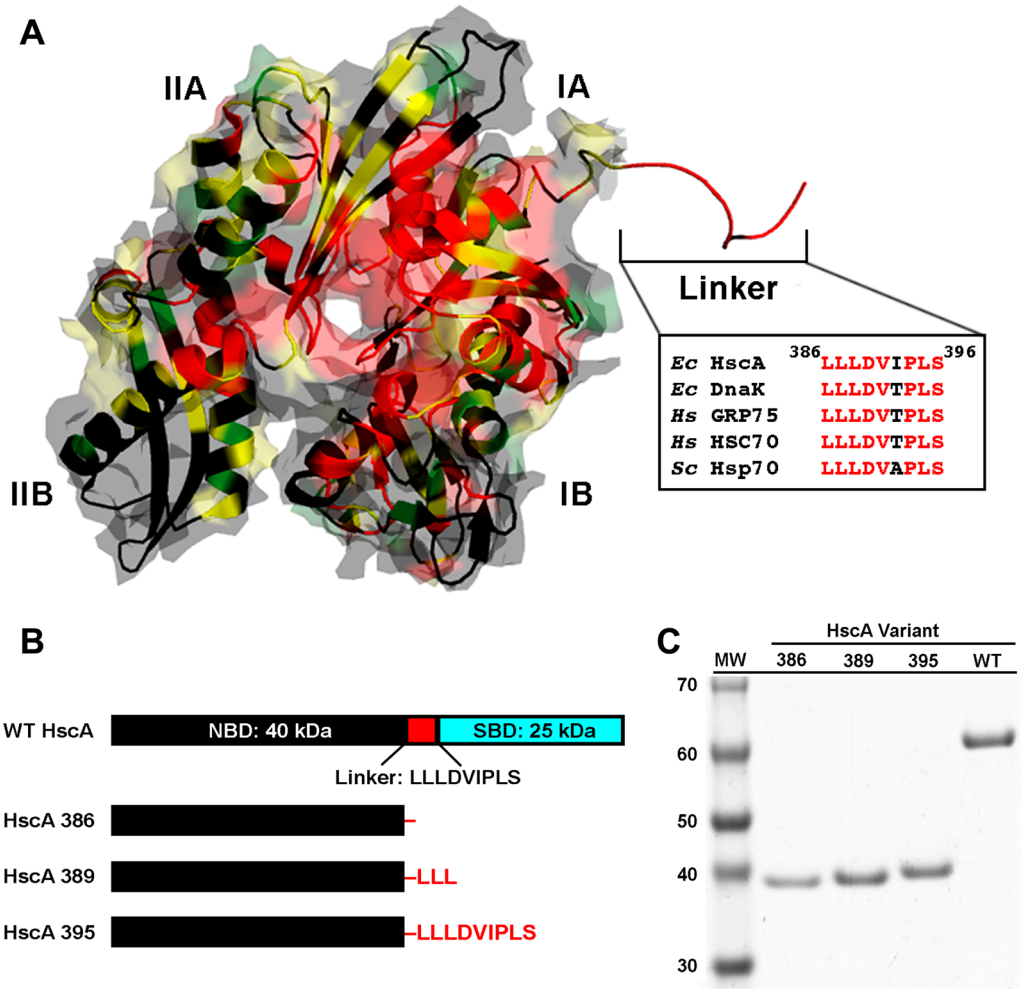

Figure 1. (A) Degree of sequence identity between DnaK and HscA mapped onto the structure of ADP-bound DnaK (PDB entry 2kho): red for identically conserved residues, yellow for highly similar residues, green for similar residues, and black for no sequence similarity. Roman numerals indicate the subdomains of DnaK's NBD; note the lack of sequence similarity in subdomain IIB where HscA's lone tryptophan is located. The highly conserved interdomain linker sequence (HscA numbering) is highlighted according to the colors noted above. Linker inset abbreviations: *Ec*, *E. coli*; *Hs*, *Homo sapiens*; *Sc*, *Saccharomyces cerevisae*. (B) Architecture of HscA and the design of variants used in this study. The sequence of the interdomain linker (truncated or otherwise) is listed next to each construct. (C) SDS−PAGE analysis of purified HscA variants. Lane 1 contains molecular weight (MW) markers with their associated MW designated at the left. Lanes 2—5 contain the respective HscA variant listed above the gel.

the homology between *E. coli* and eukaryotic ISC assembly proteins, results from studies on bacterial ISC proteins often can be translated to the human system.

In *E. coli*, the protein components necessary to synthesize and transfer Fe−S clusters are encoded by the *isc* operon.[11] Among these proteins is HscA, a specialized Hsp70-type chaperone (66 kDa) that catalyzes Fe−S cluster transfer from the scaffold protein IscU to an acceptor apo-Fe−S-protein in an ATP-dependent reaction.[12] Similar to DnaK, the general Hsp70 chaperone in *E. coli*, HscA contains a 40 kDa nucleotide-binding domain (NBD) that binds to and hydrolyzes ATP,[13,14] but its 25 kDa substrate-binding domain (SBD) uniquely recognizes a central LPPVK motif in IscU as the substrate.[15−18] Furthermore, numerous kinetic differences exist between the ATPase cycles of HscA and DnaK (Table S1 of the Supporting Information, with references therein): compared to DnaK, HscA displays a 10^3-fold weaker binding affinity for ATP, an augmented rate of ATP association, and a >10^3-fold higher rate of ADP dissociation.[19] Uniquely, and in contrast to DnaK and most Hsp70s, HscA does not require a nucleotide-exchange factor (NEF) to reset its ATPase cycle.[20,21]

Similar to that of other Hsp70s, nucleotide binding in the NBD of HscA allosterically regulates substrate (IscU) binding affinity in its SBD, with ATP-HscA (K_d^{IscU} = 37 μM) exhibiting an IscU binding affinity weaker than that of ADP-HscA (K_d^{IscU} = 1.6 μM).[22] HscB, an Hsp40-type cochaperone, binds to and delivers [2Fe-2S]-IscU to the SBD of HscA; together, IscU and HscB synergistically enhance HscA's ATPase activity nearly 1000-fold,[20,22] much like the synergistic activation observed in DnaK by DnaJ and substrate peptides. We have previously shown that IscU exists in two slowly interconverting,[23−25] metamorphic conformations, one more structured (S-state) and one more dynamically disordered (D-state), and its binding partners preferentially interact with one state over the other: HscA binds preferentially to the D-state, while HscB binds preferentially to the S-state.[26,27] Hydrolysis of bound ATP to ADP alters the conformation of HscA to the form that binds the D-state of IscU, promoting concomitant release of the [2Fe-2S] cluster from holo-IscU. Inhibition of ATP hydrolysis

dx.doi.org/10.1021/bi5010552 | *Biochemistry* 2014, 53, 7148−7159

in HscA (via an ATPase deficient mutant, HscA T212V) abolishes [2Fe-2S] cluster transfer,[12] and inactivation of the *hscA* gene leads to diminished cellular growth rates and activities of Fe−S proteins, including succinate dehydrogenase[28] and aconitase.[29]

HscA is thus vital to the maturation of Fe−S proteins, yet the structural basis of its unique nucleotide binding and dissociation features has remained unresolved, for no atomic-level information about HscA's NBD has been reported. Moreover, whereas studies of DnaK (*E. coli*) and Hsc70 (*Bos taurus* cDNA that was expressed in and purified from *E. coli*) have demonstrated that the linker modulates interdomain communication and serves as a switch that activates ATP hydrolysis,[30−33] the question whether this holds true for HscA, which relies on ATP hydrolysis to transfer [2Fe-2S] clusters from holo-IscU to recipient apo-Fe−S proteins, remains.[12] Thus, we sought to investigate the specific role of HscA's interdomain linker in an effort to probe the mechanism by which HscA catalyzes ATP hydrolysis to promote Fe−S cluster transfer.

Here, we report detailed information about the isolated NBD of HscA and how the presence of a shortened linker or full-length linker peptide affects its functional properties. We also explore the effect of adding a synthetic peptide with the sequence of the full-length linker on the properties of the isolated NDB.

MATERIALS AND METHODS

Design of NBD Variants. No high-resolution structural information exists for full-length HscA or its isolated NBD; however, numerous structures of Hsp70 homologs have been determined in various substrate- and nucleotide-bound states.[34−38] Therefore, to create variants of the HscA NBD containing a partial or full interdomain linker, we utilized structures of ADP- and ATP-bound DnaK (PDB entries 2kho and 4jne, respectively) and a bioinformatics approach to identify conserved linker residues among various Hsp70s.[35,36] Eight of the nine residues in HscA's interdomain linker sequence (L^{387}LLDVIPLS^{395}) are conserved with DnaK (*E. coli*), GRP75 (*Homo sapiens*), HSC70 (*H. sapiens*), and Hsp70 (*Saccharomyces cerevisiae*) (Figure 1A). Moreover, because actin and DnaK NBD share only ∼10% sequence homology yet both structures display similar folds characteristic of the actin/hexokinase superfamily,[39] we hypothesized that prior structural and functional studies of DnaK would be relevant to HscA, which shares 42.4% sequence homology with DnaK (Figure 1A).

Within the wild-type (WT) HscA-encoding pTrc plasmid,[14] stop codons were introduced at L^{387}, D^{390}, and L^{396} to create $HscA_{386}$ (isolated NBD), $HscA_{389}$ (NBD with a truncated linker; $L^{387}LL^{389}$ motif), and $HscA_{395}$ (NBD with a full linker; L^{387}LLDVIPLS^{395}), respectively (Figure 1B).

Protein Production. The QuikChange II site-directed mutagenesis kit (Agilent) was used to create the HscA NBD constructs mentioned above by introducing appropriate stop codons at HscA residues 387, 390, and 396 in the WT pTrc(HscA) vector,[14] and these mutations were verified with DNA sequencing. RosettaBlue(DE3) competent cells were transformed with the mutated pTrc(HscA) expression plasmids and selectively grown on medium plates containing 100 μg/mL ampicillin. For the production of unlabeled protein, cell cultures were grown in 1 L of LB medium until the optical density reached ∼1.0, upon which IPTG was added to a final concentration of 0.4 mM. Protein expression continued for 4 h, after which cells were harvested and frozen at −80 °C until they were used. For the production of [U-^{15}N]$HscA_{386}$(T212V) and [U-^{15}N]$HscA_{386}$, cells were grown in 1 L of M9 minimal medium with 100 μg/mL ampicillin and 1 g/L $^{15}NH_4Cl$. Protein expression occurred as described above. Unlabeled IscU and HscB samples were prepared as described previously.[24]

Protein Purification. To purify HscA NBD samples, anion-exchange chromatography was performed using a DEAE Bio-Gel column equilibrated with 50 mM Tris-HCl (pH 7.5), 0.5 mM EDTA, and 1.0 mM DTT (TED) buffer. Protein elution occurred over a 0 to 0.25 M NaCl gradient, and fractions containing HscA NBDs of interest were identified via SDS−PAGE. HscA-containing fractions were concentrated and subsequently subjected to size-exclusion chromatography on a HiLoad 16/60 Superdex 75 column (GE Healthcare). Protein was eluted in TED buffer supplemented with 150 mM NaCl. The concentration of HscA NBDs was determined by recording the absorbance at 280 nm in a 1 cm path-length cuvette with a theoretical extinction coefficient of 17420 M^{-1} cm^{-1}. Full-length HscA samples were purified and quantified as described previously, except that the reversed-phase size-exclusion chromatography step was eliminated.[14] The purified samples of HscA variants were analyzed for purity via SDS−PAGE (Figure 1C) and mass spectrometry (data not shown).

Synthetic Peptide. A peptide corresponding to HscA residues L^{387}LLDVIPLS^{395} was synthesized at the University of Wisconsin—Madison Biotechnology Center. It was partially dissolved in TED buffer [without DMSO (see below)] for the acquisition of NMR data at an upper limit concentration of 3 mM or HMKD buffer with 10% DMSO (v/v) and added to final concentrations of 5, 10, 50, 100, 150, 200, and 500 μM ATPase assays to ensure solubility. Above this linker peptide concentration, more DMSO was required to maintain the solubility; however, the resultant increase in the level of DMSO inhibited the ATPase activity of $HscA_{386}$, and we were unable to pursue soluble peptide concentrations above 500 μM.

ATPase Assays. To quantify the rate of ATP hydrolysis for each HscA variant, steady-state assays were conducted at 25 °C in HMKD buffer [50 mM HEPES (pH 7.3), 150 mM KCl, 10 mM $MgCl_2$, and 1 mM DTT] containing 1 μM HscA and 1 mM ATP as previously reported.[19] A standard curve of known P_i concentrations versus the respective absorbance at 360 nm was generated to determine experimental ATPase activities of HscA variants. ATPase reactions were conducted with three or more replicates, and ATPase rates were calculated by continuously monitoring the amount of phosphate released using the enzyme-coupled EnzChek Phosphate Assay Kit (Molecular Probes, Life Technologies). To determine the Michaelis−Menten constants (K_m) of $HscA_{386}$ and $HscA_{395}$, we added ATP to final concentrations of 2, 4, 10, 40, 100, and 1000 μM and plotted the resultant ATPase activities versus ATP concentration. Reactions were conducted with three replicates, and data were plotted as the mean ATPase activity for each ATP concentration. Using nonlinear regression analyses, the resultant curves were fit to the Michaelis−Menten equation to yield K_m and V_{max} values.

NMR Spectroscopy. Solution NMR solvents contained either HMKD or TED buffer (with 10 mM $MgCl_2$ and 150 mM NaCl), 7% D_2O, 0.02% sodium azide, and nucleotide or peptide, as required. Multidimensional NMR data were processed with NMRPipe[65] and visualized with Sparky.[66] For

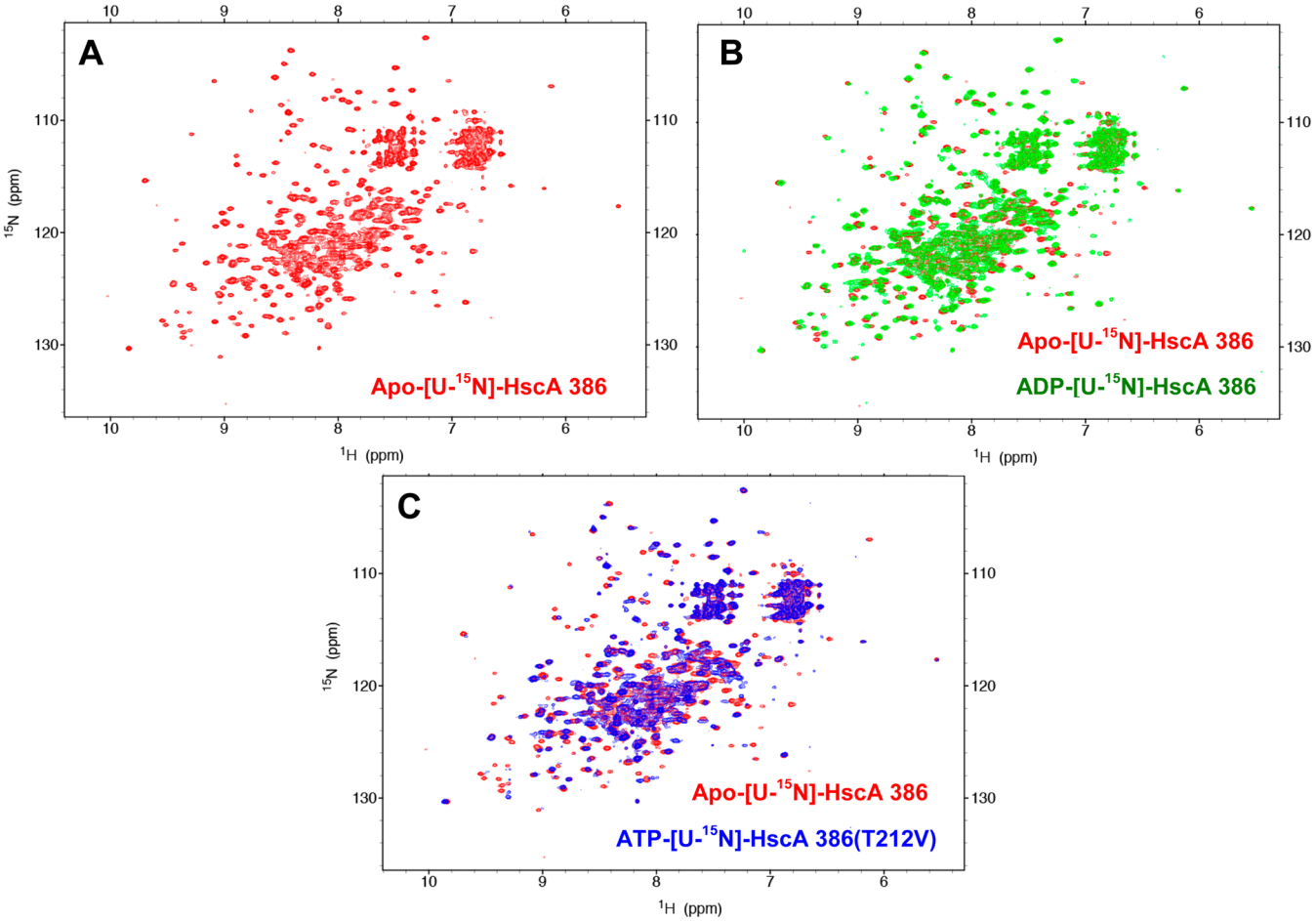

Figure 2. NMR spectroscopic investigation of nucleotide binding in $HscA_{386}$ and $HscA_{386}$(T212V). (A) 2D $^{1}H-^{15}N$ TROSY-HSQC spectrum of 0.3 mM [U-^{15}N]apo-$HscA_{386}$ in HMKD buffer (red). (B) 2D $^{1}H-^{15}N$ TROSY-HSQC spectrum of 0.3 mM [U-^{15}N]$HscA_{386}$ in HMKD buffer with 10 mM ADP (green) overlaid upon the spectrum from panel A. (C) 2D $^{1}H-^{15}N$ TROSY-HSQC spectrum of 0.3 mM [U-^{15}N]$HscA_{386}$(T212V) in HMKD buffer with 10 mM ATP (blue) overlaid upon the spectrum from panel A.

the acquisition of nucleotide binding data, [U-^{15}N]-$HscA_{386}$(T212V) was added to a final concentration of 0.3 mM. ATP or ADP was added in excess (10 mM), and spectra were acquired at 25 °C with an 800 MHz Agilent Unity-Inova spectrometer. For the acquisition of linker binding data, [U-^{15}N]$HscA_{386}$ was added to a concentration of 0.2 mM, and the synthetic linker peptide was added to a final concentration of 3 mM in TED buffer; spectra were acquired with a 900 MHz Agilent Unity-Inova spectrometer equipped with a cryogenic probe.

Intrinsic Tryptophan Fluorescence. HscA NBD samples containing 1 μM protein in HMKD buffer were excited at 295 nm, and fluorescence emission was monitored from 305 to 400 nm. As HscA contains only one tryptophan residue in its NBD (W291), the relative fluorescence emission could be directly compared between $HscA_{386}$ and $HscA_{395}$. Background fluorescence was corrected for by subtracting fluorescence from an equivalent volume of solvent alone, and fluorescence data for each sample were collected at least three times to ensure their validity. Data were acquired with a QM-1 fluorometer (Photon Technology International) with 2 nm slits, and the results were visualized with FELIX.

Differential Scanning Fluorimetry. Individual wells of a 96-well plate were filled in triplicate with 20 μL of a solution containing 2 μM protein in 5 mM HEPES buffer (pH 7.3), 10 mM $MgCl_2$, 10 mM KCl, and 10 μM SYPRO Orange dye. A ViiA 7 real-time polymerase chain reaction (PCR) instrument was employed with Protein Thermal Shift software (Life Technologies) to conduct thermal denaturation assays over a temperature range of 15−99 °C. SYPRO Orange dye was excited at 492 nm, and fluorescence emission was detected at 610 nm. The melting temperature (T_m) for each sample was determined by quantifying the temperature at which the first derivative of fluorescence emission reached a minimal value (Protein Thermal Shift software). However, for the sake of visual clarity, plots were made of the fluorescence emission versus temperature.

RESULTS

Characterization of HscA Nucleotide-Binding Domain Variants. To ensure that HscA's isolated NBD had folded properly and was able to bind to both ADP and ATP, we prepared [U-^{15}N]$HscA_{386}$(T212V), which included a previously identified mutation (T212V) that renders HscA unable to cleave ATP but still responsive to ATP-induced conformational changes observed in WT HscA,[12] and collected 2D $^{1}H-^{15}N$ TROSY-HSQC spectra in the absence of nucleotide (Figure 2A), with excess ADP (Figure 2B), and with excess ATP (Figure 2C). Vast dispersion of ^{1}H chemical shifts (Figure 2A) indicated that the NBD had folded properly, and differences in

dx.doi.org/10.1021/bi5010552 | Biochemistry 2014, 53, 7148−7159

the positions of cross-peaks in spectra of ADP-bound (Figure 2B) and ATP-bound [U-^{15}N]HscA$_{386}$(T212V) (Figure 2C) suggested that the NBD undergoes a nucleotide-induced structural rearrangement between two (or more) states, as reported in prior solution-state NMR spectroscopic[30,40−42] (but not X-ray crystallographic)[37,38] studies of DnaK. Furthermore, because the cross-peaks in the 2D ^{1}H−^{15}N TROSY-HSQC spectrum of [U-^{15}N]apo-HscA$_{386}$(T212V) in the absence of added nucleotide did not correspond to the positions of cross-peaks in spectra of the protein following the addition or ADP or ATP (Figure 2B,C), we concluded that our purified NBD likely exists in the apo state.

As found with other Hsp70s,[38,43] binding of nucleotide to the NBD of HscA was dependent on the presence of Mg^{2+}: the 2D ^{1}H−^{15}N TROSY-HSQC spectra of apo and ATP-bound [U-^{15}N]HscA$_{386}$(T212V) were nearly superimposable when they were acquired in TED buffer that lacked Mg^{2+} (Figure S1 of the Supporting Information). Thus, all subsequent structural and functional assays involving ATP were conducted in HKMD buffer, which contained 10 mM $MgCl_2$.

HscA's Interdomain Linker Autoactivates ATP Hydrolysis but Does Not Confer Sensitivity to HscB-Mediated Stimulation of ATPase Activity. Silberg et al.[13] had previously analyzed the ATPase activity of HscA's isolated NBD, but because the variant used in the study was truncated at residue 382, the potential ATPase-activating role of the interdomain linker was left unexplored. We characterized the ATPase activity of each HscA NBD variant (Figure 3A) by using a steady-state spectrophotometric assay that couples the hydrolysis of ATP to the enzymatic conversion of 2-amino-6-mercapto-7-methylpurine riboside (MESG) to ribose 1-phosphate and 2-amino-6-mercapto-7-methylpurine via purine nucleoside phosphorylase (PNP). By adding 1 mM ATP to a solution containing 1 μM HscA and following the change in absorbance at 360 nm, we could directly quantify the amount of ATP hydrolyzed per minute per mole of ATPase (ATPase activity, reported in units of min^{-1}) over time. As shown in panels A and B of Figure 3, the steady-state ATPase activity of HscA$_{395}$ (V_{max}^{395} = 0.443 min^{-1}) was 13-fold higher than that of HscA$_{386}$ (V_{max}^{386} = 0.0352 min^{-1}) and 17-fold higher than that of WT HscA (V_{max}^{WT} = 0.0254 min^{-1}), whereas HscA$_{389}$ (V_{max}^{389} = 0.230 min^{-1}), which contains only the highly conserved L^{387}LL^{389} motif, exhibited 7- and 9-fold increases in its respective ATPase activity. Moreover, HscA$_{395}$ autoactivated ATP hydrolysis to rates that exceeded those of WT HscA stimulated by a 50-fold molar excess of HscB ($V_{max}^{WT+HscB}$ = 0.288 min^{-1}) or IscU ($V_{max}^{WT+IscU}$ = 0.257 min^{-1}) (Figure 3B), HscA's cochaperone or substrate, respectively. As expected, the addition of 50 μM IscU had no effect on the ATPase activities of any of the NBD variants (Figure 3B), because they all lack the SBD that interacts with IscU. Collectively, these results are consistent with previous investigations of DnaK[30,31] and Hsc70[32] and illustrate the conserved role of the Hsp70 interdomain linker in autoactivating ATP hydrolysis, even in this specialized Hsp70-type chaperone dedicated to Fe−S cluster transfer.

Reports on the matter of ATPase stimulation of isolated Hsp70 NBDs in the presence of their Hsp40 cochaperones have differed.[31,32] An NMR investigation by Greene et al.[44] confirmed that DnaK's isolated NBD was able to bind to DnaJ's isolated J-domain in solution, but the interaction failed to stimulate its ATPase activity.[31] On the other hand, the ATPase activity of Hsc70 NBDs was found to be stimulated by its J-protein (auxilin) if and only if the interdomain linker was present.[32] Here, we investigated the effects imparted by HscB (the Hsp40 cochaperone) on the ATPase activities of WT HscA and the three HscA NBD variants. In agreement with previously published data,[45,46] the ATPase activity of 1 μM WT HscA increased by a factor of 8 in the presence of 50 μM HscB (Figure 3B). However, similar 50:1 HscB:HscA$_{386}$, HscB:HscA$_{389}$, or HscB:HscA$_{395}$ molar ratios did not elicit any stimulation of ATPase activity (Figure 3B).

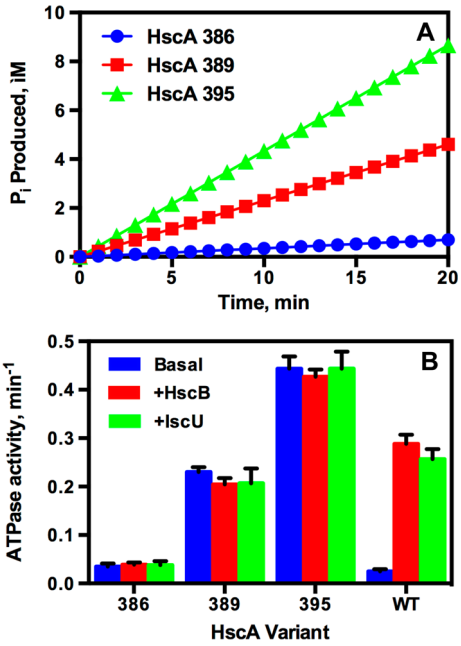

Figure 3. (A) Steady-state kinetics of ATP hydrolysis in HscA NBD variants measured spectrophotometrically. Production of inorganic phosphate (P$_i$) via ATP hydrolysis was directly proportional to the absorbance at 360 nm. Each sample contained 1 μM protein in HKMD buffer at 25 °C. The interdomain linker (HscA$_{395}$, green diamonds) enhanced HscA's basal ATPase activity 13-fold in comparison to that of the isolated NBD (HscA$_{386}$, blue circles). The highly conserved L^{387}LL^{389} motif in the linker (HscA$_{389}$, red squares) was sufficient to autoactivate ATP hydrolysis to rates that were 7-fold faster than those of HscA$_{386}$. Mean ATPase activities are plotted here (n = 3) vs time. (B) ATPase activities of HscA$_{386}$, HscA$_{389}$, HscA$_{395}$, and WT HscA alone (blue) and in the presence of a 50-fold molar excess of HscB (red) or under IscU-stimulated conditions (green). The ATPase activities of all three NDB variants were not affected by added HscB or IscU. By contrast, the ATPase activity of WT HscA was enhanced in the presence of HscB or IscU. The presence of the SBD in WT HscA serves to decrease the activity of the NDB under all conditions studied. The Y-axis units are reported as moles of ATP hydrolyzed per mole of HscA per minute, or turnover number. Error bars are the standard deviation (n = 3).

HscA's Interdomain Linker Binds to Its NBD in the *cis* Configuration, Altering the Fluorescence Emission and ^{1}H NMR Line Width of W291 and Enhancing the Inherent Thermostability of the NBD. Given the clear role of the linker in autoactivating ATP hydrolysis, we collected 2D ^{1}H−^{15}N TROSY-HSQC spectra of 0.3 mM apo-[U-^{15}N]-HscA$_{386}$ and 0.3 mM apo-[U-^{15}N]HscA$_{395}$ in HMKD buffer to investigate potential linker−NBD interactions in the apo state. In the spectrum of apo-[U-^{15}N]HscA$_{395}$, additional cross-peaks arose from linker residues, as expected; however, approximately 20 cross-peaks either experienced severe line broadening and were rendered undetectable or were significantly displaced from

dx.doi.org/10.1021/bi5010552 | Biochemistry 2014, 53, 7148−7159

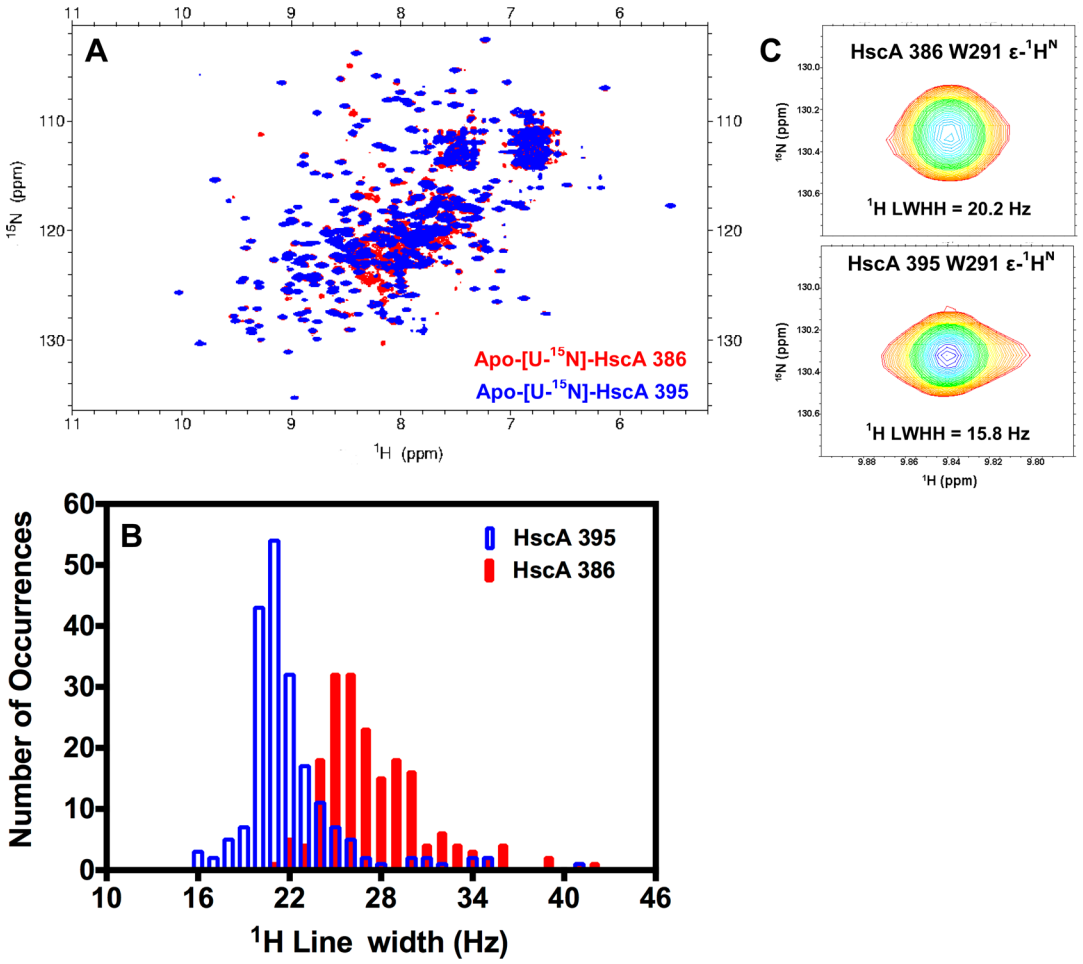

Figure 4. NMR spectra of apo-[U-^{15}N]HscA$_{386}$ and apo-[U-^{15}N]HscA$_{395}$ indicate a binding interaction in the linker's *cis* configuration. (A) Overlay of 2D ^{1}H−^{15}N TROSY-HSQC spectra of 0.3 mM apo-[U-^{15}N]HscA$_{386}$ (red) and 0.3 mM apo-[U-^{15}N]HscA$_{395}$ (blue) acquired at 900 MHz in HMKD buffer. (B) Distribution of ^{1}H line widths at half peak height (LWHH) measured from 200 well-resolved peaks in the spectra presented in panel A. ^{1}H LWHH values from apo-[U-^{15}N]HscA$_{386}$ are colored red, and ^{1}H LWHH values from apo-[U-^{15}N]HscA$_{395}$ are outlined in blue. The mean ^{1}H LWHH values for apo-[U-^{15}N]HscA$_{386}$ and apo-[U-^{15}N]HscA$_{395}$ are 27.2 ± 4.5 and 21.6 ± 3.3 Hz, respectively, with errors representing one standard deviation. (C) Comparison of the ^{1}H LWHH of the cross-peak arising from the ε-^{1}H^{N} on the side chain of W291. Spectra in panel A were used for this analysis. Peak contours have been colored on a red to blue spectrum to indicate intensity.

their respective positions in the corresponding spectrum of apo-[U-^{15}N]HscA$_{386}$ (Figure 4A). This finding suggests that the linker interacts with a distinct subset of NBD residues. Moreover, linker−NBD interactions in HscA$_{395}$ significantly altered the distribution of ^{1}H line widths at half-height (LWHH) calculated from ∼200 well-resolved, nonoverlapping peaks in the 2D ^{1}H−^{15}N TROSY-HSQC spectra. The mean ^{1}H LWHH values were 27.2 ± 4.5 Hz for apo-[U-^{15}N]HscA$_{386}$ and 21.6 ± 3.3 Hz for apo-[U-^{15}N]HscA$_{395}$ (Figure 4B).

To further investigate the nucleotide-independent linker−NBD interactions, we utilized two fluorescence assays: an intrinsic tryptophan fluorescence assay that has been used to characterize structural rearrangements in DnaK[47,48] and a differential scanning fluorimetry (DSF) thermal denaturation/fluorescence assay that reports on intrinsic protein stability.[49] We probed the tryptophan fluorescence emission profiles of HscA$_{386}$ and HscA$_{395}$ to examine the local chemical environment of W291, the lone tryptophan residue in HscA's NBD (Figure 5A). HscA$_{395}$ displayed a red-shifted, enhanced fluorescence profile (λ_{max} = 329 nm) in comparison to that of HscA$_{386}$ (λ_{max} = 326 nm) (Figure 5A), suggesting that the apo-NBD−linker interaction causes W291 to become more exposed to solvent, in concordance with our NMR data presented above. The LWHH values for the ^{1}H$^{\varepsilon 1}$ of W291 in apo-HscA$_{395}$ and apo-HscA$_{386}$ were 15.8 and 20.2 Hz, respectively (Figure 4C), which suggested that W291 becomes more dynamic or exposed to solvent in apo-HscA$_{395}$. In HscA$_{395}$, the normalized peak intensity of the W291 side chain ^{1}H^{N} was modestly increased (∼10%) over that of HscA$_{386}$ (data not shown), indicating enhanced motions on the nanosecond time scale.

Next, HscA$_{386}$ and HscA$_{395}$ were subjected to heat denaturation in the presence of a dye (SYPRO Orange) that fluoresces (excitation at 492 nm and emission at 610 nm) upon binding to hydrophobic patches of unfolded proteins. Thus, the fluorescence signal intensity is directly proportional to the amount of unfolded protein in a given sample, and protein melting temperatures (T_m) are extracted from the lowest point in the first-derivative plot of fluorescence intensity.[49] Protein aggregation at higher temperatures often results in a decay of the fluorescence signal.[49] As seen in Figure 5B, HscA$_{395}$ melted at 54.35 °C whereas HscA$_{386}$ melted at 49.25 °C, indicating that the interactions between the NBD and interdomain linker confer enhanced basal thermostability to the NBD. These

dx.doi.org/10.1021/bi5010552 | *Biochemistry* 2014, 53, 7148−7159

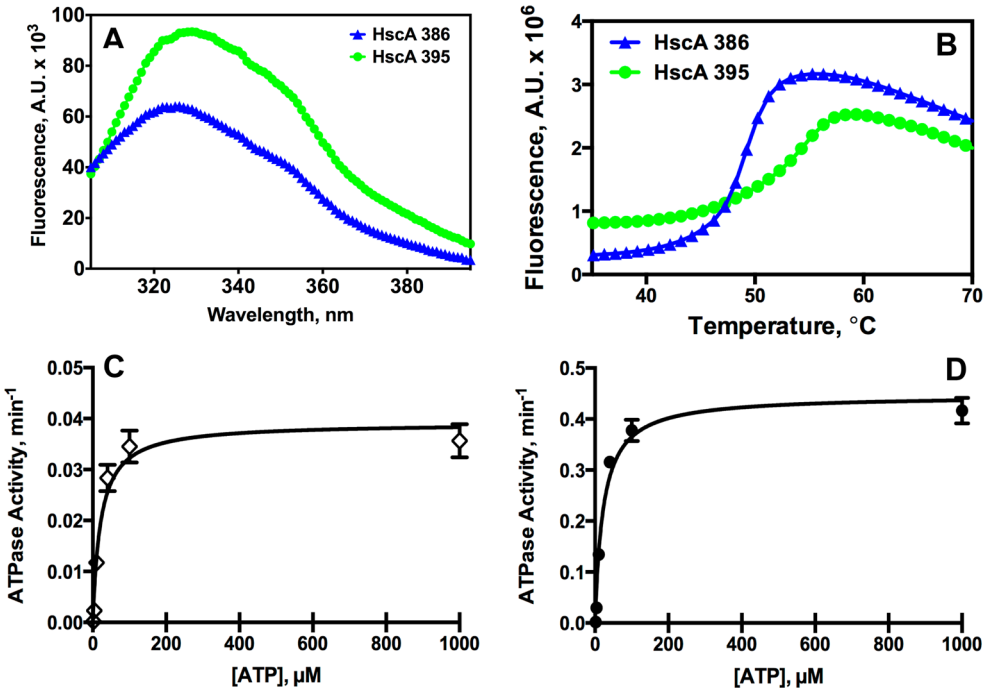

Figure 5. Direct comparison of $HscA_{386}$ and $HscA_{395}$ by intrinsic tryptophan fluorescence, DSF, and enzyme kinetics. (A) Intrinsic tryptophan fluorescence traces of $HscA_{386}$ and $HscA_{395}$. HscA's lone tryptophan residue (W291) is located on a β-sheet near the bottom of sub-domain IIB, which is known to rotate by ≥14° in DnaK but does not share much sequence homology with HscA in comparison to other NBD subdomains. Note the enhanced emission and red-shifted λ_{max} in $HscA_{395}$. (B) Differential scanning fluorimetry (DSF) thermal melting curves for $HscA_{386}$ and $HscA_{395}$. The melting temperature (T_m) of $HscA_{386}$ was 49.25 °C, which was significantly lower than that of $HscA_{395}$ (54.35 °C), suggesting that the linker confers thermostability by binding to the NBD. The melting temperatures (n = 3 for $HscA_{386}$, and n = 3 for $HscA_{395}$) of each replicate were identical. (C and D) ATPase activity plotted as a function of ATP concentration for (C) $HscA_{386}$ (◇) and (D) $HscA_{395}$ (●). Note that the values of K_m for $HscA_{386}$ (21.4 ± 4.0 μM) and $HscA_{395}$ (22.8 ± 3.2 μM) are very similar to the K_d^{ATP} (26 ± 7 μM) and K_m (12.6 μM) of WT HscA. Thus, the linker has no effect on apparent ATP binding affinity, but rather on catalytic activity (V_{max}^{386} = 0.039 ± 0.001 min^{-1}; V_{max}^{395} = 0.446 ± 0.016 min^{-1}). Results are shown with error bars for the standard deviation (n = 3).

results are consistent with our Trp fluorescence data (Figure 5A), which suggested that the linker binds to the NBD, as well as with results from a thermal denaturation study via circular dichroism in which the T_m of $DnaK_{392}$ (DnaK NBD and the LLL of the linker) was 3.5 °C higher than that of $DnaK_{388}$ (the isolated DnaK NBD).[30]

The Presence or Absence of the Interdomain Linker Does Not Affect the Apparent ATP Binding Affinity of the NBD. To examine whether linker−NBD interactions enhance the NBD's binding affinity for ATP, we conducted ATPase assays as a function of ATP concentration while holding the HscA concentration constant (Figure 5C,D). From comparison of the Michaelis−Menten (K_m) constants determined for $HscA_{386}$ (K_m^{386} = 21.4 ± 4.0 μM) and $HscA_{395}$ (K_m^{395} = 22.8 ± 3.2 μM), it was readily apparent that the interdomain linker has no effect on the apparent ATP binding affinity. Moreover, both K_m^{386} and K_m^{395} are similar to binding affinity constants previously determined for WT HscA: K_d^{ATP} (26 ± 7 μM) and K_m (12.6 μM).[19] This further indicates that the interdomain linker does not play a role in ATP binding but rather increases the catalytic rate of ATP hydrolysis (V_{max}^{386} = 0.039 ± 0.001 min^{-1}; V_{max}^{395} = 0.446 ± 0.016 min^{-1}).

The Synthetic HscA Linker Peptide (LLLDVIPLS) Binds to the Isolated NBD and Stimulates ATP Hydrolysis in the *trans* Configuration. 2D $^1H-^{15}N$ TROSY-HSQC spectra of 0.2 mM [U-^{15}N]$HscA_{386}$ were collected in the absence and presence of a 15-fold molar excess of the linker peptide, which was partially dissolved in TED buffer to avoid complications with excess DMSO (see Materials and Methods and Figure S2 of the Supporting Information). The presence of the peptide led to widespread chemical shift perturbations, including distinct broadening of some signals (Figure 6A, bottom right inset), indicative of protein−ligand interactions (Figure 6A). A concentration dependence was observed in the fold stimulation of the ATPase activity of 1 μM $HscA_{386}$ upon addition of increasing amounts of linker peptide [5−500 μM (Figure S2 of the Supporting Information)] dissolved in HMKD buffer with 10% (v/v) DMSO. Maximal ATPase activity reached nearly 4-fold over basal levels (Figure 6B), after which the peptide required higher DMSO concentrations to fully dissolve. The enhanced concentration of DMSO in turn disrupted the basal ATPase activity of apo-$HscA_{386}$ (data not shown), and therefore, we were unable to pursue higher linker peptide concentrations to quantitatively determine the K_m value.

$HscA_{395}$ hydrolyzed ATP at a rate that was 3-fold faster than that of $HscA_{386}$ in the presence of 500 μM linker peptide (Figure 2B). This incomplete stimulation of ATPase activity likely results from relatively weaker binding interactions between the NBD and linker peptide in the *trans* configuration ($HscA_{386}$ and peptide) as compared to the *cis* ($HscA_{395}$) configuration. Indeed, a comparison of the 2D $^1H-^{15}N$ TROSY-HSQC spectra of apo-[U-^{15}N]$HscA_{395}$ in TED buffer and [U-^{15}N]$HscA_{386}$ in the presence of 3 mM linker peptide, which corresponds to a 15-fold molar excess, indicates that unique cross-peaks appear in the spectrum of linker-bound $HscA_{386}$ (Figure S3 of the Supporting Information). Nevertheless, identical *cis*- and *trans*-linker-induced chemical shift perturbations and a decrease in the ^1H LWHH of ε-$^1H^N$ of

dx.doi.org/10.1021/bi5010552 | *Biochemistry* 2014, 53, 7148−7159

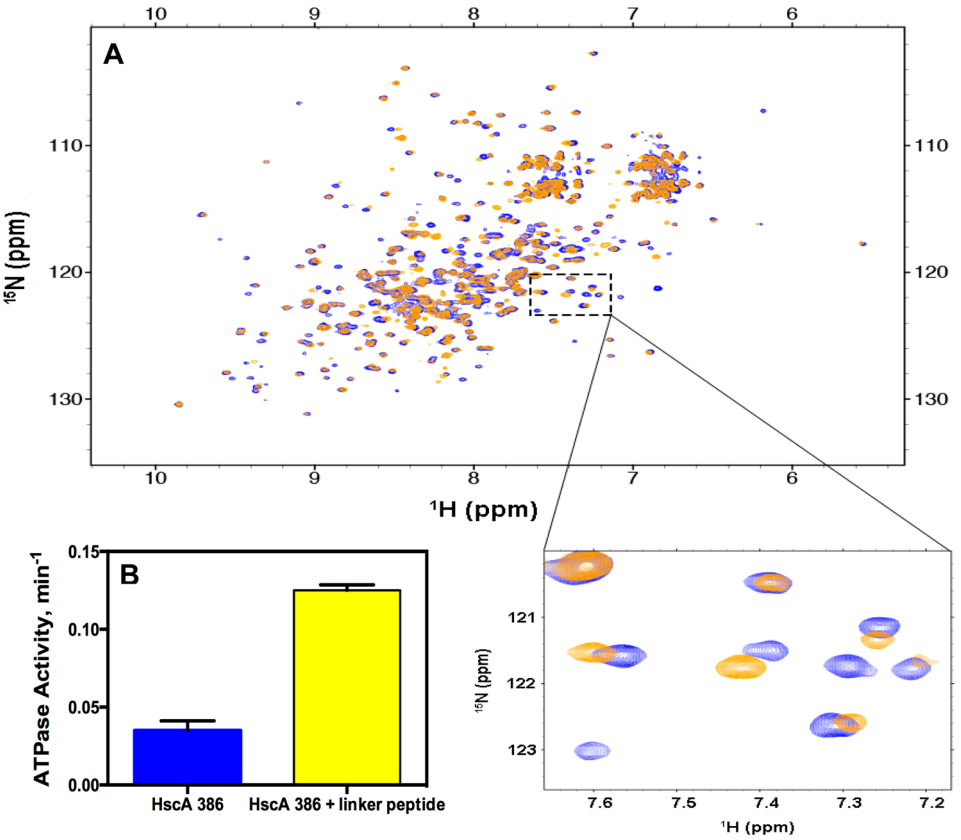

Figure 6. (A) 2D ^{1}H−^{15}N TROSY-HSQC spectra of [U-^{15}N]HscA$_{386}$ at a final concentration of 0.2 mM in the absence (blue) and presence (orange) of a 15-fold molar excess of interdomain linker peptide (LLLDVIPLS) partially dissolved in TED buffer. Spectra were acquired at 900 MHz. (B) Steady-state ATPase assays conducted under conditions identical to those described in the legend of Figure 3 (except for the addition of linker peptide). Addition of 0.5 mM peptide increased the ATPase activity of the isolated NBD by a factor of nearly 4. See Figure S2 of the Supporting Information for a linker peptide concentration titration.

W291 (20.4 Hz in apo-HscA$_{386}$ vs 16.7 Hz in linker peptide-bound HscA$_{386}$ under identical buffer conditions) are apparent (Figure S3 of the Supporting Information), suggesting that the observed binding between the NBD and synthetic linker peptide does not emerge from nonspecific interactions.

DISCUSSION

Chaperone Action in the Crowded *in Vivo* Environment. Hsp70s function, among other roles, to ensure that nascent polypeptides fold properly into their correct conformations, that endocytosed clathrin-coated vesicles are unassembled, and that organelle-targeted proteins arrive at the proper translocase machinery.[50−53] Misfolded and unfolded proteins are recognized by the cochaperone Hsp40 and escorted to Hsp70's SBD, which binds to solvent-exposed hydrophobic residues and allows abnormally folded proteins to refold into their native conformations.[52] Owing to such diverse and indispensable roles, Hsp70 is among the most highly conserved proteins, and many eukaryotic and prokaryotic genomes encode multiple Hsp70s: e.g., humans have 13 Hsp70s dispersed among the cellular compartments for various roles.[54]

High-Resolution Structures of DnaK Bound to ADP and ATP Provide Insight into Hsp70 Function. High-resolution structures of full-length DnaK, the canonical Hsp70 chaperone of *E. coli*, bound to ADP[36] and ATP[35] (Figure S4 of the Supporting Information) have provided mechanistic insight into DnaK's allosteric interdomain communication. Numerous studies have established that substrate binding stimulates ATPase activity in DnaK's NBD and thereby creates a mechanism that efficiently utilizes energy derived from ATP hydrolysis to conduct polypeptide refolding or other proteostatic functions.[60] Crystal structures of isolated DnaK NBDs in various nucleotide states have failed to capture the delicate intersubdomain allostery that modulates substrate binding affinity,[37,38] whereas solution-state NMR spectroscopic studies have instead demonstrated that ATP or ADP binding significantly alters NBD subdomain orientation and flexibility.[30,41−43] In the NMR structure of ADP-DnaK, the NBD and SBD are joined by a flexible linker and appear to be relatively independent of one another; they each retain structures similar to those of their isolated domains.[36] Mutations in the linker have been shown to disrupt chaperone action via compromised interdomain communication and cochaperone recognition.[31,32,55−57] DnaK's interdomain linker is therefore critical to interdomain allostery and serves as a connection between ATP binding in the NBD and substrate binding affinity in the SBD.[32,33,35,39,58,59]

Role of the Interdomain Linker in HscA Compared to That in DnaK and Hsc70. The results reported here allow us to compare the role of the interdomain linker in HscA, an Hsp70 specialized for Fe−S cluster biosynthesis in *E. coli*, with prior results from other Hsp70s (i.e., *E. coli* DnaK and bovine Hsc70 purified from *E. coli*). Evaluation of the steady-state ATPase activities of the HscA NBD variants shows that the linker autoactivates ATP hydrolysis in the NBD (Figure 3A),

dx.doi.org/10.1021/bi5010552 | *Biochemistry* 2014, 53, 7148−7159

with basal rates that exceed the rate of HscB- or IscU-mediated stimulation of WT HscA (Figure 3B). These findings are consistent with previously published studies of DnaK and Hsc70[30−32] that illustrated the conserved role of the interdomain linker in autostimulating ATPase activity. Additionally, the apparent ATP binding affinities of $HscA_{395}$ and $HscA_{386}$ were identical within experimental error (Figure 5C,D), indicating that the linker is primarily involved in catalyzing the cleavage of ATP. Moreover, the average ^1H LWHH in apo-$HscA_{395}$ (21.6 ± 3.3 Hz) was significantly more narrow than that in apo-$HscA_{386}$ (27.2 ± 4.5 Hz) (Figure 4B); as line broadening can result from, among other contributions, chemical exchange that is intermediate on the NMR time scale, it is possible that apo-$HscA_{386}$ adopts a variety of conformations in solution, whereas linker−NBD interactions in apo-$HscA_{395}$ select for one conformer or a subset of conformers. Elegant NMR studies of the NBD of DnaK have demonstrated that this ATPase domain transmits its allosteric signals via conformational selection, with apo- and ADP-DnaK NBD adopting a variety of conformations in solution. Spin relaxation experiments in combination with resonance assignments of HscA will be required to investigate this possibility in more detail.

In $HscA_{395}$, the interdomain linker enhances fluorescence emission from W291 (Figure 5A) and increases basal thermostability in comparison to that of $HscA_{386}$ (Figure 5B), suggesting that the linker interacts with the NBD in the absence of a nucleotide. Furthermore, the ^1H line width of the side chain $^1H^N$ in W291 has become narrower in $HscA_{395}$, which indicates enhanced mobility. This finding is not entirely inconsistent with prior data from investigations of DnaK, wherein Gierasch and co-workers reported that the truncated linker ($DnaK_{392}$) was highly flexible and dynamic in the apo state;[30] however, small perturbations to peak intensities and backbone chemical shifts were observed in nucleotide-free $DnaK_{392}$.[30,33] Moreover, linker−NBD interactions in a two-domain DnaK construct, while primarily nucleotide-dependent, were similarly found to occur in the apoprotein.[59] However, fluorescence results with HscA presented herein cannot be compared directly to similar measurements on DnaK, because the tryptophan of DnaK (W102) studied by fluorescence is 43 Å from the residue corresponding to W291 (M296) in ADP-DnaK (Figure S5 of the Supporting Information). M296 resides on a β-strand near the bottom of subdomain IIB that is known to rotate by 14° during DnaK's ATPase cycle,[61] perhaps indicating that this region in HscA is sensitive to linker−NBD interactions.

Activation of ATP Hydrolysis by the Interdomain Linker. Our ATPase assays illustrate that the SBD of HscA represses basal ATPase activity by restricting the linker's access to the NBD. This internal inhibition likely functions to couple ATP hydrolysis in the NBD to the binding of HscB and [2Fe-2S]-IscU, interactions that presumably remodel HscA's tertiary structure to allow the linker to dock onto the NBD and activate ATP hydrolysis. Such a mechanism would ensure that HscA efficiently utilizes energy derived from ATP hydrolysis to specifically transfer [2Fe-2S] clusters. Silberg et al.[19] previously characterized ATP binding in HscA through an absorbance assay, demonstrating that ATP binding occurs in two steps: a fast ATP binding event and a slow ATP-induced conformational change. Because ATP binding is also known to destabilize HscA−peptide complexes,[13,16] the binding of ATP and consequent activation of ATP hydrolysis exquisitely regulate the formation and dissociation of [2Fe-2S]-IscU−HscB−HscA ternary complexes and resultant [2Fe-2S] cluster transfer.

Through extensive structural and biochemical studies, DnaK's linker was determined to play a key role in interdomain allostery.[33,55,59,62] Across all Hsp70s, the interdomain linker displays nearly ubiquitous conservation of its internal hydrophobic sequence (LLLDV-PL) with some variation of residue identity at the N- and C-termini. In the NMR structure of ADP- and peptide-bound DnaK, the interdomain linker (V^{389}LLLDVTPLS^{398}, DnaK numbering) was found to be highly dynamic and was not observed in the NMR spectra,[36] yet in the ATP-bound crystal structure, the linker had docked onto the NBD and adopted a β-sheet conformation.[35] Prior NMR analyses of $DnaK_{392}$ had identified docking of the truncated linker ($V^{389}LLL^{392}$),[30,33] which was sensitive to nucleotide binding and consistent with other structural analyses of the full-length protein.[39] Moreover, this indicated that the presence of the SBD restricted the ability of the linker to dock onto the NBD (i.e., the NBD and SBD were essentially isolated domains in ADP-DnaK, but coupled in ATP-DnaK) and activate ATP hydrolysis. We observed a similar SBD-mediated repression of ATP hydrolysis in our investigation of HscA NBD variants (Figure 3B). We speculate that stimulation of HscA's ATPase activity by HscB and IscU results from enhanced linker−NBD interactions that are not present or occur with diminished probabilities in the unstimulated full-length protein.

HscB Does Not Stimulate the ATPase Activity of HscA's NBD with or without the Interdomain Linker. By examining the ATPase activity of HscA NBD variants in the presence of excess HscB, we determined that neither the isolated NBD ($HscA_{386}$) nor the NBD with a full interdomain liker ($HscA_{395}$) was receptive to ATPase stimulation via HscB (Figure 3B). A recent NMR study from our lab demonstrated that the interaction between HscB and ATP-bound HscA NBD lacked vital contacts with HscB's J-domain.[63] Full-length HscA was found to be sensitive to HscB-mediated activation of ATPase activity through ATP-dependent interactions with the J-domain of HscB.[63] From these results, it was unclear whether the linker plays a role in HscB-mediated activation of ATP hydrolysis. Here, we have shown that HscA's linker alone is not sufficient; thus, the presence of the SBD is required to elicit a functional activation from HscB. However, the mechanism by which the SBD facilitates activation of ATPase stimulation by HscB remains unclear: does the SBD in ATP-HscA optimally position the NBD and linker for interaction with HscB, or does the SBD itself contact HscB and facilitate subsequent activation of ATP hydrolysis? Elucidation of the HscB-binding interface on ATP-HscA will help answer this question.

Our results are consistent with a prior investigation of DnaK−DnaJ interactions, which similarly showed that DnaK's SBD is required for ATPase stimulation by DnaJ.[56] However, Jiang et al.[32] demonstrated that the ATPase activity of an Hsc70 NBD variant with a truncated linker could be stimulated by its J-protein, auxilin. Similar results were not seen with the Hsc70 isolated NBD, suggesting that linker−auxilin interactions were primarily responsible for ATPase activation by auxilin.[32] Differences between these studies may arise from mechanistic distinctions between auxilin and DnaJ or HscB, or from functional disparities between Hsc70 and DnaK or HscA. Indeed, the NBD and SBD in Hsc70 are known to contact one another in the apo and ADP states,[32,64] whereas DnaK's NBD and SBD remain relatively isolated and free from contact under these conditions.[30,36] Determining how the two domains of

HscA interact under various nucleotide conditions will shed light on this apparent mechanistic distinction among Hsp70s.

Effects of Adding a Non-Covalent Linker to $HscA_{386}$. By using solution-state NMR spectroscopy, we found that a peptide corresponding to HscA's interdomain linker (L^{387}LLVIDPLS^{395}) interacts with $HscA_{386}$ in the absence of nucleotide (Figure 6A), and our ATPase assays demonstrated that this synthetic linker peptide stimulates the ATPase activity of the isolated NBD nearly 4-fold over basal levels (Figure 6B). Narrowing of the W291 ε-$^{1}H^{N}$ line width in $HscA_{386}$ in the presence of the linker peptide (16.7 Hz; 20.4 Hz in apo-$HscA_{386}$ under identical buffer conditions) further confirms the specificity and WT-like binding interactions (Figure S3 of the Supporting Information) in the *trans* configuration.

As compared to the 2D $^{1}H-^{15}N$ TROSY-HSQC spectrum of [U-^{15}N]$HscA_{395}$, both identical and unique chemical shift perturbations appear in the 2D $^{1}H-^{15}N$ TROSY-HSQC spectrum of [U-^{15}N]$HscA_{386}$ in the presence of the linker peptide (Figure S3 of the Supporting Information). On one hand, this indicates that the linker peptide, while interacting with the NBD in a native-like manner, could also impart non-native NBD conformations. On the other hand, these unique *trans* linker configuration signals could also arise from native-like interactions that are unsaturated by the weakly binding linker peptide. Without complete backbone resonance assignments, however, interpretation of these spectra remains challenging, as no residue-specific information (other than the side chain of W291) can be obtained regarding a comparison of the linker-binding site in *cis* and *trans* configurations.

Nonetheless, this is the first indication that an exogenously added Hsp70 linker peptide can bind to its isolated NBD and stimulate ATP hydrolysis in the *trans* configuration (Figure 6B), presenting the unique ability to isotopically label individual residues within the linker for NMR or IR spectroscopic structural and functional studies. This system could prove useful in dissecting the structural and dynamical roles of specific interdomain linker residues upon binding to ATP-bound NBD versus apo-NBD. Prior NBD−linker investigations relied on selective labeling of individual amino acid types (e.g., ^{15}N-labeled leucine residues in ref 30) or distinct chemical moieties (e.g., protonated, ^{13}C-labeled methyl groups in an otherwise deuterated background in ref 59). Here, we offer the ability to further probe the roles of interdomain linker residues via solid-state peptide synthesis with any combination of isotopic labels.

■ ASSOCIATED CONTENT

Supporting Information

Structures of ATP- and ADP-bound DnaK, a comparison of the kinetic parameters in the ATPase cycles of DnaK and HscA, NMR spectra that highlight the essential role of Mg^{2+} in facilitating binding of ATP to HscA's NBD, NMR spectra that compare the effects of linker binding in *cis* and *trans* configurations, and HscA NBD ATPase assays as a function of added linker peptide concentration. This material is available free of charge via the Internet at http://pubs.acs.org.

■ AUTHOR INFORMATION

Corresponding Author

*E-mail: jmarkley@wisc.edu. Phone: (608) 263-9349. Fax: (608) 262-1759.

Present Addresses

[‖]T.R.A.: Physical and Theoretical Chemistry Laboratory, Department of Chemistry, University of Oxford, Oxford, U.K. [⊥]J.H.K.: Max Planck Institute for Biophysical Chemistry, Göttingen, Germany.

Funding

This work was supported by National Institutes of Health (NIH) Grant U01 GM94622 and made use of the National Magnetic Resonance Facility at Madison, which is funded by NIH Grant P41GM66326 (National Institute of General Medical Sciences). Equipment was purchased with funds from the University of Wisconsin—Madison, the NIH (P41RR02301, P41GM66326, S10RR02781, S10RR08438, S10RR023438, S10RR025062, and S10RR029220), the National Science Foundation (DMB-8415048, OIA-9977486, and BIR-9214394), and the U.S. Department of Agriculture.

Notes

The authors declare no competing financial interest.

■ ACKNOWLEDGMENTS

We thank Dr. Jung Ho Lee (Laboratory of Chemical Physics, National Institutes of Health, Bethesda, MD) for assistance with purifying [U-^{15}N]$HscA_{395}$, Dr. David Aceti (Center for Eukaryotic Structural Genomics, University of Wisconsin—Madison) for generously providing training on the ViiA 7 RT-PCR instrument for use in DSF thermal melts, and William Ford Freyberg for critically reading the manuscript and providing helpful feedback.

■ ABBREVIATIONS

2D, two-dimensional; AU, arbitrary units; DnaK, stress-inducible heat shock protein 70 kDa (Hsp70) in *E. coli*; DSF, differential scanning fluorimetry; DTT, dithiothreitol; HKMD, 50 mM HEPES (pH 7.3), 150 mM KCl, 10 mM $MgCl_2$, and 1 mM DTT; $HscA_{386}$, isolated nucleotide-binding domain (NBD) of HscA; $HscA_{389}$, NBD of HscA containing a short (three-amino acid) linker peptide; $HscA_{395}$, NBD of HscA containing the full-length (nine-amino acid) linker peptide; Hsc70, constitutively expressed heat shock cognate 70 kDa (*B. taurus*) purified from *E. coli*; HSQC, heteronuclear single-quantum coherence; NBD, nucleotide-binding domain; PCR, polymerase chain reaction; PDB, Protein Data Bank; P_i, inorganic phosphate; ROS, reactive oxygen species; SBD, substrate-binding domain; SDS−PAGE, sodium dodecyl sulfate−polyacrylamide gel electrophoresis; TED, 50 mM Tris-HCl (pH 7.5), 0.5 mM EDTA, and 1 mM DTT; TROSY, transverse relaxation-optimized spectroscopy; [U-], uniformly labeled.

■ REFERENCES

(1) Beinert, H., Holm, R. H., and Münck, E. (1997) Iron-sulfur clusters: Nature's modular, multipurpose structures. *Science 277*, 653−659.

(2) Lill, R. (2009) Function and biogenesis of iron-sulphur proteins. *Nature 460*, 831−838.

(3) Lill, R., and Mühlenhoff, U. (2008) Maturation of iron-sulfur proteins in eukaryotes: Mechanisms, connected processes, and diseases. *Annu. Rev. Biochem. 77*, 669−700.

(4) Johnson, D. C., Dean, D. R., Smith, A. D., and Johnson, M. K. (2005) Structure, function, and formation of biological iron-sulfur clusters. *Annu. Rev. Biochem. 74*, 247−281.

(5) Imlay, J. A. (2006) Iron-sulphur clusters and the problem with oxygen. *Mol. Microbiol. 59*, 1073−1082.

(6) Lill, R., Hoffmann, B., Molik, S., Pierik, A. J., Rietzschel, N., Stehling, O., Uzarska, M. A., Webert, H., Wilbrecht, C., and Mühlenhoff, U. (2013) The role of mitochondria in cellular iron-sulfur protein biogenesis and iron metabolism. *Biochim. Biophys. Acta 1823*, 1491−1508.
(7) Rouault, T. A. (2012) Biogenesis of iron-sulfur clusters in mammalian cells: New insights and relevance to human disease. *Dis. Models & Mech. 5*, 155−164.
(8) Sheftel, A., Stehling, O., and Lill, R. (2010) Iron-sulfur proteins in health and disease. *Trends Endocrinol. Metab. 21*, 302−314.
(9) Isaya, G. (2014) Mitochondrial iron-sulfur cluster dysfunction in neurodegenerative disease. *Front. Pharmacol. 5*, 29.
(10) Markley, J. L., Kim, J. H., Dai, Z., Bothe, J. R., Cai, K., Frederick, R. O., and Tonelli, M. (2013) Metamorphic protein IscU alternates conformations in the course of its role as the scaffold protein for iron-sulfur cluster biosynthesis and delivery. *FEBS Lett. 587*, 1172−1179.
(11) Zheng, L., Cash, V. L., Flint, D. H., and Dean, D. R. (1998) Assembly of iron-sulfur clusters. Identification of an iscSUA-hscBA-fdx gene cluster from *Azotobacter vinelandii*. *J. Biol. Chem. 273*, 13264−13272.
(12) Bonomi, F., Iametti, S., Morleo, A., Ta, D., and Vickery, L. E. (2008) Studies on the mechanism of catalysis of iron-sulfur cluster transfer from IscU[2Fe2S] by HscA/HscB chaperones. *Biochemistry 47*, 12795−12801.
(13) Silberg, J. J., Hoff, K. G., Tapley, T. L., and Vickery, L. E. (2001) The Fe/S assembly protein IscU behaves as a substrate for the molecular chaperone Hsc66 from *Escherichia coli*. *J. Biol. Chem. 276*, 1696−1700.
(14) Vickery, L. E., Silberg, J. J., and Ta, D. T. (1997) Hsc66 and Hsc20, a new heat shock cognate molecular chaperone system from *Escherichia coli*. *Protein Sci. 6*, 1047−1056.
(15) Tapley, T. L., and Vickery, L. E. (2004) Preferential substrate binding orientation by the molecular chaperone HscA. *J. Biol. Chem. 279*, 28435−28442.
(16) Hoff, K. G., Ta, D. T., Tapley, T. L., Silberg, J. J., and Vickery, L. E. (2002) Hsc66 substrate specificity is directed toward a discrete region of the iron-sulfur cluster template protein IscU. *J. Biol. Chem. 277*, 27353−27359.
(17) Hoff, K. G., Cupp-Vickery, J. R., and Vickery, L. E. (2003) Contributions of the LPPVK motif of the iron-sulfur template protein IscU to interactions with the Hsc66-Hsc20 chaperone system. *J. Biol. Chem. 278*, 37582−37589.
(18) Cupp-Vickery, J. R., Peterson, J. C., Ta, D. T., and Vickery, L. E. (2004) Crystal structure of the molecular chaperone HscA substrate binding domain complexed with the IscU recognition peptide ELPPVKIHC. *J. Mol. Biol. 342*, 1265−1278.
(19) Silberg, J. J., and Vickery, L. E. (2000) Kinetic characterization of the ATPase cycle of the molecular chaperone Hsc66 from *Escherichia coli*. *J. Biol. Chem. 275*, 7779−7786.
(20) Vickery, L. E., and Cupp-Vickery, J. R. (2007) Molecular chaperones HscA/Ssq1 and HscB/Jac1 and their roles in iron-sulfur protein maturation. *Crit. Rev. Biochem. Mol. Biol. 42*, 95−111.
(21) Silberg, J. J., Hoff, K. G., and Vickery, L. E. (1998) The Hsc66-Hsc20 chaperone system in *Escherichia coli*: Chaperone activity and interactions with the DnaK-DnaJ-grpE system. *J. Bacteriol. 180*, 6617−6624.
(22) Hoff, K. G., Silberg, J. J., and Vickery, L. E. (2000) Interaction of the iron-sulfur cluster assembly protein IscU with the Hsc66/Hsc20 molecular chaperone system of *Escherichia coli*. *Proc. Natl. Acad. Sci. U.S.A. 97*, 7790−7795.
(23) Kim, J. H., Tonelli, M., Kim, T., and Markley, J. L. (2012) Three-Dimensional Structure and Determinants of Stability of the Iron-Sulfur Cluster Scaffold Protein IscU from *Escherichia coli*. *Biochemistry 51*, 5557−5563.
(24) Kim, J. H., Füzéry, A. K., Tonelli, M., Ta, D. T., Westler, W. M., Vickery, L. E., and Markley, J. L. (2009) Structure and dynamics of the iron-sulfur cluster assembly scaffold protein IscU and its interaction with the cochaperone HscB. *Biochemistry 48*, 6062−6071.
(25) Dai, Z., Tonelli, M., and Markley, J. L. (2012) Metamorphic protein IscU changes conformation by cis-trans isomerizations of two peptidyl-prolyl peptide bonds. *Biochemistry 51*, 9595−9602.
(26) Kim, J. H., Tonelli, M., Frederick, R. O., Chow, D. C., and Markley, J. L. (2012) Specialized Hsp70 chaperone (HscA) binds preferentially to the disordered form, whereas J-protein (HscB) binds preferentially to the structured form of the iron-sulfur cluster scaffold protein (IscU). *J. Biol. Chem. 287*, 31406−31413.
(27) Cai, K., Frederick, R. O., Kim, J. H., Reinen, N. M., Tonelli, M., and Markley, J. L. (2013) Human mitochondrial chaperone (mtHSP70) and cysteine desulfurase (NFS1) bind preferentially to the disordered conformation, whereas co-chaperone (HSC20) binds to the structured conformation of the iron-sulfur cluster scaffold protein (ISCU). *J. Biol. Chem. 288*, 28755−28770.
(28) Tokumoto, U., and Takahashi, Y. (2001) Genetic analysis of the *isc* operon in *Escherichia coli* involved in the biogenesis of cellular iron-sulfur proteins. *J. Biochem. 130*, 63−71.
(29) Johnson, D. C., Unciuleac, M. C., and Dean, D. R. (2006) Controlled expression and functional analysis of iron-sulfur cluster biosynthetic components within *Azotobacter vinelandii*. *J. Bacteriol. 188*, 7551−7561.
(30) Swain, J. F., Dinler, G., Sivendran, R., Montgomery, D. L., Stotz, M., and Gierasch, L. M. (2007) Hsp70 chaperone ligands control domain association via an allosteric mechanism mediated by the interdomain linker. *Mol. Cell 26*, 27−39.
(31) Vogel, M., Mayer, M. P., and Bukau, B. (2006) Allosteric regulation of Hsp70 chaperones involves a conserved interdomain linker. *J. Biol. Chem. 281*, 38705−38711.
(32) Jiang, J., Maes, E. G., Taylor, A. B., Wang, L., Hinck, A. P., Lafer, E. M., and Sousa, R. (2007) Structural basis of J cochaperone binding and regulation of Hsp70. *Mol. Cell 28*, 422−433.
(33) Zhuravleva, A., and Gierasch, L. M. (2011) Allosteric signal transmission in the nucleotide-binding domain of 70-kDa heat shock protein (Hsp70) molecular chaperones. *Proc. Natl. Acad. Sci. U.S.A. 108*, 6987−6992.
(34) Mayer, M. P. (2013) Hsp70 chaperone dynamics and molecular mechanism. *Trends Biochem. Sci. 38*, 507−514.
(35) Qi, R., Sarbeng, E. B., Liu, Q., Le, K. Q., Xu, X., Xu, H., Yang, J., Wong, J. L., Vorvis, C., Hendrickson, W. A., Zhou, L., and Liu, Q. (2013) Allosteric opening of the polypeptide-binding site when an Hsp70 binds ATP. *Nat. Struct. Mol. Biol. 20*, 900−907.
(36) Bertelsen, E. B., Chang, L., Gestwicki, J. E., and Zuiderweg, E. R. (2009) Solution conformation of wild-type *E. coli* Hsp70 (DnaK) chaperone complexed with ADP and substrate. *Proc. Natl. Acad. Sci. U.S.A. 106*, 8471−8476.
(37) Flaherty, K. M., DeLuca-Flaherty, C., and McKay, D. B. (1990) Three-dimensional structure of the ATPase fragment of a 70K heat-shock cognate protein. *Nature 346*, 623−628.
(38) Flaherty, K. M., Wilbanks, S. M., DeLuca-Flaherty, C., and McKay, D. B. (1994) Structural basis of the 70-kilodalton heat shock cognate protein ATP hydrolytic activity. II. Structure of the active site with ADP or ATP bound to wild type and mutant ATPase fragment. *J. Biol. Chem. 269*, 12899−12907.
(39) Zuiderweg, E. R., Bertelsen, E. B., Rousaki, A., Mayer, M. P., Gestwicki, J. E., and Ahmad, A. (2013) Allostery in the Hsp70 chaperone proteins. *Top. Curr. Chem. 328*, 99−153.
(40) Revington, M., Holder, T. M., and Zuiderweg, E. R. (2004) NMR study of nucleotide-induced changes in the nucleotide binding domain of *Thermus thermophilus* Hsp70 chaperone DnaK: Implications for the allosteric mechanism. *J. Biol. Chem. 279*, 33958−33967.
(41) Revington, M., Zhang, Y., Yip, G. N., Kurochkin, A. V., and Zuiderweg, E. R. (2005) NMR investigations of allosteric processes in a two-domain *Thermus thermophilus* Hsp70 molecular chaperone. *J. Mol. Biol. 349*, 163−183.
(42) Bhattacharya, A., Kurochkin, A. V., Yip, G. N., Zhang, Y., Bertelsen, E. B., and Zuiderweg, E. R. (2009) Allostery in Hsp70 chaperones is transduced by subdomain rotations. *J. Mol. Biol. 388*, 475−490.

(43) Wilbanks, S. M., DeLuca-Flaherty, C., and McKay, D. B. (1994) Structural basis of the 70-kilodalton heat shock cognate protein ATP hydrolytic activity. I. Kinetic analyses of active site mutants. *J. Biol. Chem. 269*, 12893−12898.
(44) Greene, M. K., Maskos, K., and Landry, S. J. (1998) Role of the J-domain in the cooperation of Hsp40 with Hsp70. *Proc. Natl. Acad. Sci. U.S.A. 95*, 6108−6113.
(45) Silberg, J. J., Tapley, T. L., Hoff, K. G., and Vickery, L. E. (2004) Regulation of the HscA ATPase reaction cycle by the co-chaperone HscB and the iron-sulfur cluster assembly protein IscU. *J. Biol. Chem. 279*, 53924−53931.
(46) Füzéry, A. K., Tonelli, M., Ta, D. T., Cornilescu, G., Vickery, L. E., and Markley, J. L. (2008) Solution structure of the iron-sulfur cluster cochaperone HscB and its binding surface for the iron-sulfur assembly scaffold protein IscU. *Biochemistry 47*, 9394−9404.
(47) Slepenkov, S. V., and Witt, S. N. (1998) Kinetics of the reactions of the *Escherichia coli* molecular chaperone DnaK with ATP: Evidence that a three-step reaction precedes ATP hydrolysis. *Biochemistry 37*, 1015−1024.
(48) Theyssen, H., Schuster, H. P., Packschies, L., Bukau, B., and Reinstein, J. (1996) The second step of ATP binding to DnaK induces peptide release. *J. Mol. Biol. 263*, 657−670.
(49) Niesen, F. H., Berglund, H., and Vedadi, M. (2007) The use of differential scanning fluorimetry to detect ligand interactions that promote protein stability. *Nat. Protoc. 2*, 2212−2221.
(50) Kim, Y. E., Hipp, M. S., Bracher, A., Hayer-Hartl, M., and Hartl, F. U. (2013) Molecular chaperone functions in protein folding and proteostasis. *Annu. Rev. Biochem. 82*, 323−355.
(51) Saibil, H. (2013) Chaperone machines for protein folding, unfolding and disaggregation. *Nat. Rev. Mol. Cell Biol. 14*, 630−642.
(52) Buchberger, A., Bukau, B., and Sommer, T. (2010) Protein quality control in the cytosol and the endoplasmic reticulum: Brothers in arms. *Mol. Cell 40*, 238−252.
(53) Bukau, B., Weissman, J., and Horwich, A. (2006) Molecular chaperones and protein quality control. *Cell 125*, 443−451.
(54) Gupta, R. S. (1998) Protein phylogenies and signature sequences: A reappraisal of evolutionary relationships among archaebacteria, eubacteria, and eukaryotes. *Microbiol. Mol. Biol. Rev. 62*, 1435−1491.
(55) Kumar, D. P., Vorvis, C., Sarbeng, E. B., Cabra Ledesma, V. C., Willis, J. E., and Liu, Q. (2011) The four hydrophobic residues on the Hsp70 inter-domain linker have two distinct roles. *J. Mol. Biol. 411*, 1099−1113.
(56) Han, W., and Christen, P. (2001) Mutations in the interdomain linker region of DnaK abolish the chaperone action of the DnaK/DnaJ/GrpE system. *FEBS Lett. 497*, 55−58.
(57) Laufen, T., Mayer, M. P., Beisel, C., Klostermeier, D., Mogk, A., Reinstein, J., and Bukau, B. (1999) Mechanism of regulation of hsp70 chaperones by DnaJ cochaperones. *Proc. Natl. Acad. Sci. U.S.A. 96*, 5452−5457.
(58) Liu, Q., and Hendrickson, W. A. (2007) Insights into Hsp70 chaperone activity from a crystal structure of the yeast Hsp110 Sse1. *Cell 131*, 106−120.
(59) Zhuravleva, A., Clerico, E. M., and Gierasch, L. M. (2012) An interdomain energetic tug-of-war creates the allosterically active state in Hsp70 molecular chaperones. *Cell 151*, 1296−1307.
(60) De Los Rios, P., and Barducci, A. (2014) Hsp70 chaperones are non-equilibrium machines that achieve ultra-affinity by energy consumption. *eLife 3*, e02218.
(61) Harrison, C. J., Hayer-Hartl, M., Di Liberto, M., Hartl, F., and Kuriyan, J. (1997) Crystal structure of the nucleotide exchange factor GrpE bound to the ATPase domain of the molecular chaperone DnaK. *Science 276*, 431−435.
(62) Vogel, M., Bukau, B., and Mayer, M. P. (2006) Allosteric regulation of Hsp70 chaperones by a proline switch. *Mol. Cell 21*, 359−367.
(63) Kim, J. H., Alderson, T. R., Frederick, R. O., and Markley, J. L. (2014) Nucleotide-dependent interactions within a specialized Hsp70/Hsp40 complex involved in Fe-S cluster biogenesis. *J. Am. Chem. Soc. 136*, 11586−11589.
(64) Jiang, J., Prasad, K., Lafer, E. M., and Sousa, R. (2005) Structural basis of interdomain communication in the Hsc70 chaperone. *Mol. Cell 20*, 513−524.
(65) Delagio, F., Grzesiek, S., Vuister, G. W., Zhu, G., Pfeifer, J., and Bax, A. (1995) NMRPipe: A multidimensional spectral processing system based on UNIX pipes. *J. Biomol. NMR 6*, 277−293.
(66) Goddard, T. D., and Kneller, D. G. (2008) *SPARKY 3*, University of California, San Francisco.

NOTE ADDED AFTER ISSUE PUBLICATION

This paper was accidentally published without the final author corrections applied. Details of the scientifically significant changes are outlined in an Addition and Correction: DOI: 10.1021/bi501490v.